Construction and Building Materials 175 (2018) 588–600

Contents lists available at ScienceDirect

Construction and Building Materials

journal homepage: www.elsevier.com/locate/conbuildmat

Special Issue
Use of NORM-containing products in construction

Influence of the addition of phosphogypsum on some properties of ceramic tiles

M. Contreras [a,*], S.R. Teixeira [b], G.T.A. Santos [b], M.J. Gázquez [a,c], M. Romero [d], J.P. Bolívar [a]

[a] Department of Integrated Sciences, University of Huelva, Campus de Excelencia Internacional del Mar (CEIMAR), 21071 Huelva, Spain
[b] Department of Physics, São Paulo State University (UNESP), FCT/DF, Presidente Prudente, São Paulo, Brazil
[c] Department of Applied Physics, Escuela de Ingeniería, Puerto Real, 11510 Cádiz, Spain
[d] Department of Construction, Instituto de Ciencias de la Construcción Eduardo Torroja (IETcc-CSIC), 28033 Madrid, Spain

HIGHLIGHTS

- The addition of phosphogypsum waste in ceramic bodies was evaluated.
- The new ceramic tiles shown even better technological properties than standards.
- No significant environmental impact and human risk on use this building material.
- The use of this waste can reduce the raw materials demands and phosphogypsum piles.

ARTICLE INFO

Article history:
Received 18 June 2017
Received in revised form 7 April 2018
Accepted 14 April 2018
Available online 3 May 2018

Keywords:
Phosphogypsum
NORM
Ceramic
Leaching
Valorisation

ABSTRACT

Phosphogypsum (PG) is a waste from phosphoric acid production, and this work evaluates the use of PG as an additive in ceramic manufacturing. Ceramic samples were produced by adding different concentrations of PG (5, 7.5, and 10 wt%) to natural clay, and sintering at 950, 1050, and 1150 °C. Technological and mechanical properties of the obtained ceramics were evaluated. Moreover, the U.S. EPA's toxicity characteristic leaching procedure, Index "I", and the effective radium activity were calculated to evaluate the environmental risks. The use of PG improves the sintering behaviour and the bending strength, while also the environmental impact is negligible.

1. Introduction

Any process that requires the use of raw materials and applies physical and/or chemical transformations to obtain products generates waste and impacts the environment. It is necessary to develop sustainable industrial processes in which the waste generated will be used as raw materials for new commercial products and applications. The industrial production of phosphoric acid (H_3PO_4) from phosphate rock ore (mainly fluorapatite, $Ca_5(PO_4)_3F$) by the wet process (using H_2SO_4) produces a gypsum-rich by-product called phosphogypsum [1–3]. The industrial process is shown by the following chemical reaction (Eq. (1)):

$$Ca_5(PO_4)_3F + 5H_2SO_4 + 10H_2O \Longleftrightarrow 3H_3PO_4 + 5(CaSO_4 \cdot 2H_2O) + HF \quad (1)$$

Nowadays, worldwide PG production is estimated at approximately 100–280 millions of tonnes per year [4,5]; 4.9 tonnes of PG are generated per tonne of phosphoric acid produced. Nevertheless, only 15% of the world's waste PG is recycled [6,7], because it often contains hazardous metals and other potentially toxic elements – even natural U-series radionuclides and organic substances [8,9].

The city of Huelva (in south-west Spain) presents the only centre of production of phosphoric acid in Spain, and the largest centre in Europe. Production began in 1968, and since then 120 million tonnes of PG has been deposited in a stack occupying a large part (1200 ha) of the salt-marshes of the Tinto River [3,10]. After looking unsuccessfully for sustainable solutions to the stockpiling of

* Corresponding author.
E-mail address: manuel.contreras@dfa.uhu.es (M. Contreras).

https://doi.org/10.1016/j.conbuildmat.2018.04.131
0950-0618/

waste, the plant ceased dumping PG in December 2010. However, the waste piles remain, and without an apparent solution. The urgent need to perform the current study is related to the great social interest for an action plan that proposes solutions to the problem of the PG stacks.

A review of the literature on the use of PG indicates that the main applications remain in agriculture, cement production, and in the construction and building industry (the object of this study). The 15% of waste PG that is successfully recycled is implemented in the creation of building materials [11–13], as a soil amendment [2], to produce Portland cement [14], in mineral CO_2 sequestration [15,16], and other applications [17].

However, it is essential that the other 85% of waste PG is reused. In other words, there is a strong need to diversify the industrial applications of this waste. Some authors have focused on recycling gypsum for traditional ceramic building materials [18], such as synthetic polymer cement [19], ceramic block [20], and non-fired ceramic [21]. The increasing amount of PG being produced, and thus the need for increasingly large storage areas such as that in the city of Huelva, have led to a considerable need for the development of new economically and environmentally attractive methods to recycle this industrial waste.

Therefore, the objective of this work is to analyse the option of producing ceramic bodies that utilise PG. Ceramics were produced with different firing temperatures and PG proportions, which were analysed in comparison to a standard red ceramic. Several studies in relation to technological properties and environmental implications were carried out.

2. Materials and methods

2.1. Materials and sample preparation

A representative sample of PG was collected directly from the piles in the city of Huelva. PG was directly collected from the pile number 2, where a representative sampling of the area was performed by taking 10 samples at 50 cm in depth trying to avoid the superficial weathering produced by the rain. In general, the variability (given as standard deviation of the mean) of the major elements, trace elements and natural radionuclides was smaller than 20%. The PG was dried at 60 °C for 48 h until constant weight (to remove moisture without losing the structural water), then ground and homogenised in a planetary mill at 400 rpm for 20 min. According to previous studies [2,3], the major components of waste PG are SO_3, CaO, F, SiO_2, and P_2O_5. The clay used in this study came from the Paraná river bank near to Presidente Epitácio county, Brazil; as determined by Teixeira et al. [22], clay is mainly composed by Al_2O_3 and SiO_2. In our case, the Brazilian clays used are kaolinitic, with a little mica and iron oxide content, being their composition very similar to the clays from Sierra de Aracena (Huelva province, Spain) [23].

Clay ceramic bodies with additions of 0, 5, 7.5, or 10 wt% of PG were moistened by spraying with distilled water (12 wt%), homogenised the samples manually (12 h), and then pressed in triplicate, utilising a uniaxial manual hydraulic press (Schuz) with a load of 19 MPa in a steel mould, to form specimens of 60 × 20 × 5 mm. The elaborated compositions are shown in Table 1. All specimens were dried at room temperature for 48 h and then at 110 °C in a laboratory oven until constant weight was achieved. The firing of the specimens was performed at different temperatures (950, 1050, and 1150 °C) in a laboratory electric furnace (EDG model 3000) at a heating rate of 10 °C min^{-1}. The temperature was held at 100 °C for 30 min to evaporate the remaining structural water, and at the maximum temperature for 1 h to ensure complete sintering. The samples are numbered C-T, where C is the wt% of PG and T is the firing temperature. For example, the sample with a 5 wt% PG addition fired at 1150 °C would be 5-1150 (Table 1).

Table 1
Composition of the different mixtures studied.

	Raw materials (wt%)	
	Clay	Phosphogypsum
Fired at 950 °C		
0-950	100	0
5-950	95	5
7.5-950	92.5	7.5
10-950	90	10
Fired at 1050 °C		
0-1050	100	0
5-1050	95	5
7.5-1050	92.5	7.5
10-1050	90	10
Fired at 1150 °C		
0-1150	100	0
5-1150	95	5
7.5-1150	92.5	7.5
10-1150	90	10

2.2. Methods

The clay texture (sand, silt, and clay fractions) was characterised using the pipette method [24] and the PG particle size was analysed by laser granulometry in wet suspension with water as dispersant, using a Malbern Mastersizer 2000 particle sizer with the Hydro 2000M accessory. The mineral phases were identified by X-ray diffraction (XRD) in a Shimadzu diffractometer (model XRD 6000), using Cu κα radiation working at 1.2 kW (40 kV and 30 mA). Data were recorded in the 5–60° 2θ range (step size equal to 1° min^{-1}). Major and trace elements were analysed by inductively coupled plasma mass spectrometry (ICP-MS) using an HP branded computer (model HP4500®) at the Activation Laboratories Ltd (ACTLABS, Ontario, Canada), which meet the ISO/IEC 17025 Quality System standard. The quality control included the use of a reagent blank, standard reference materials, and replicates. The average accuracy of the analytical data was ±5%.

Thermogravimetric analysis (TGA) of the powder samples (particle size 80–100 μm) was simultaneously conducted in a TA Instruments thermogravimetric analyser with differential scanning calorimeter (TGA-DSC, model SDT Q600). Thermogravimetric scans were performed between 25 °C and 1450 °C at 10 °C min^{-1} in flowing air, using platinum crucibles with calcined Al_2O_3 as a reference material. The DSC/TGA curves were normalised regarding the sample weight.

The sintering behaviour of the fired specimens, for each composition and temperature, was tested according to the bulk density (BD), apparent porosity (AP), and water absorption (WA) according to standard procedures ISO 10545-3 [25] and ASTM C373-14 [26]. The BD (g cm^{-3}) was measured by dividing the dry mass by the external volume; the AP (%) was calculated by dividing the internal volume by the external volume; and the WA (%) was determined by dividing the internal volume by the dry mass. Moreover, linear shrinkage (LS) was calculated using the standard method ASTM C326-9 [27]. The LS was obtained by measurements of the samples before and after the firing stage using a digital calliper (Mitutoyo, precision of ±0.01 mm). The technological properties were evaluated by bending strength (BS), determined in a Contenco testing machine (model UMC-20T) according to ISO 10545-4 [28] and ASTM C674-13 [29]. Moreover, a triplicate analysis was performed in order to evaluate the repeatability and reference specimens

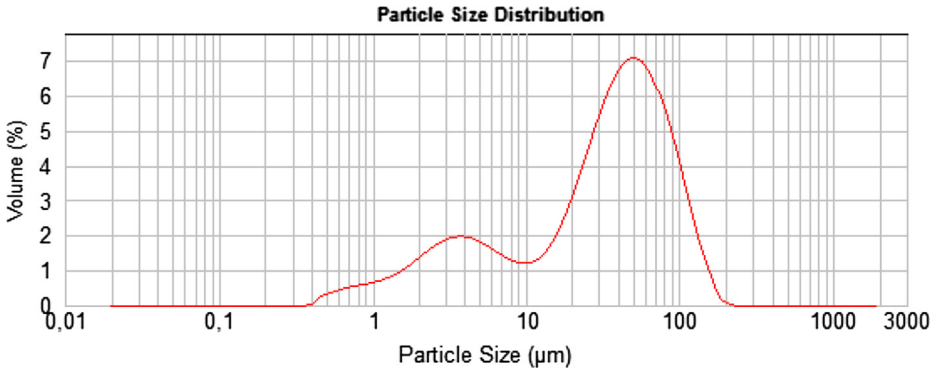

Fig. 1. Granulometric analysis of phosphogypsum.

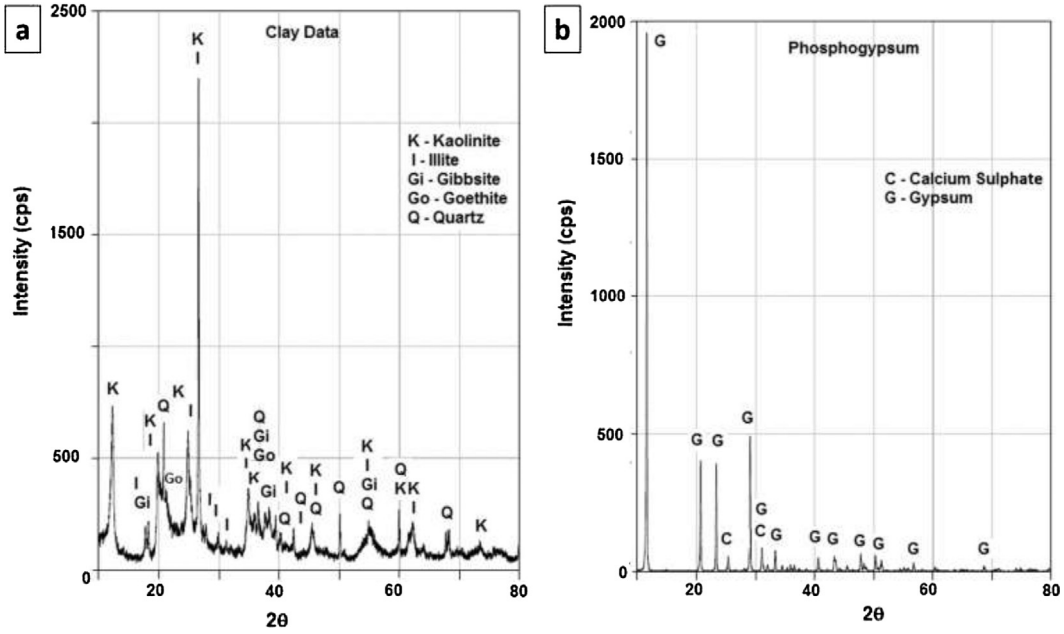

Fig. 2. XRD analysis of the raw materials: (a) clay pattern and (b) phosphogypsum pattern.

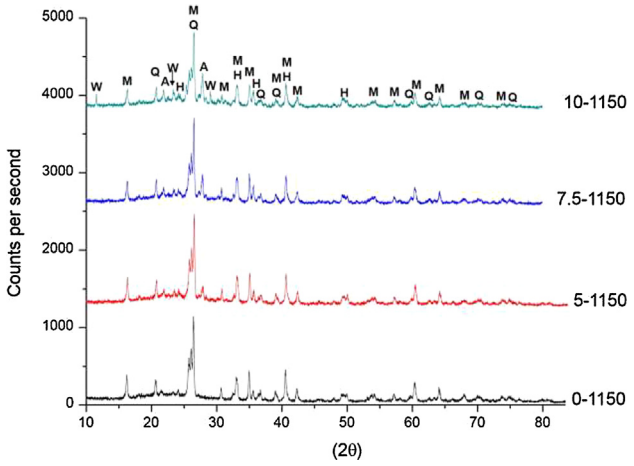

Fig. 3. XRD patterns super-impose of the fired materials at 1150 °C: M – mullite, Q – quartz; W – wallastonite, H – hematite; A – anorthite.

were used, and for that, all technological properties are expressed with their standard uncertainties.

Field emission scanning electron microscopy (FESEM) observations on fired samples were accomplished in a HITACHI S-4800P microscope with an acceleration voltage of 20 kV. For analysis of phase assemblages and morphology, fresh fracture surfaces were etched for 4 min in 15% HF solution then washed ultrasonically with distilled water and ethylic alcohol and dried. Moreover, to analyse the porosity evolution during firing, cross-sectional samples were grinded with SiC powder and subsequently polished to 1 μm with diamond pastes. Prior to FESEM observations, the samples were coated with Au-Pd in a Balzers SCD 050 sputter. The semi-quantitative analysis of different phases was achieved by energy dispersive X-ray spectroscopy (EDS) with a Link eXL detector provided by a beryllium (Be) window. The distribution of Si, Al, Ca, and Fe among different crystalline phases was examined by digital X-ray mapping.

According to the regulations of the Environmental Protection Agency (EPA), PG is considered hazardous. To study the pollutant mobility in both the raw materials and ceramic bodies, the EPA's

Table 2
Chemical concentrations analysis of major elements (wt%) and trace elements (mg kg^{-1}) of the raw materials (clay and PG) and the different mixtures measured by ICP-MS.

	SiO_2 (%)	Na_2O (%)	SO_3 (%)	MgO (%)	P_2O_5 (%)	Al_2O_3 (%)	K_2O (%)	CaO (%)	Fe_2O_3 (%)	Cr (ppm)	Mn (ppm)	Ni (ppm)	Co (ppm)	Zn (ppm)	As (ppm)	Zr (ppm)	Cu (ppm)	Sr (ppm)	Pb (ppm)
Clay	48.82	0.16	0.02	0.84	0.05	27.67	2.55	0.25	7.09	93.1	256	69.8	20.1	144	1.1	164	177	62.5	35.1
PG	0.61	0.03	52.2	<0.01	0.33	0.15	0.03	30.58	0.08	20.8	6	3.2	<0.1	5.8	<0.1	4	8.1	325	5.2
0-950	46.14	0.18	0.02	0.74	0.05	27.90	2.66	0.22	7.15	205	263	78.2	22.1	153	4.0	208	141	54.2	39
10-950	40.92	0.17	1.9	0.78	0.09	23.46	2.41	4.17	7.28	168	267	70.5	20.2	119	3.6	194	110	120	35.8
0-1150	45.33	0.19	0.02	0.99	0.03	28.15	3.00	0.28	8.31	211	302	80.7	23.4	145	1.9	126	171	67.2	39.9
5-1150	43.22	0.19	1.23	0.99	0.05	26.13	2.98	2.4	8.37	179	292	78.7	23.1	145	1.7	123	173	96	39.6
7.5-1150	40.12	0.20	1.99	0.97	0.06	24.87	2.89	3.65	7.99	167	292	76.8	22.2	113	0.9	113	107	109	41.4
10-1150	39.95	0.20	2.3	0.94	0.08	20.60	2.87	4.82	8.30	168	300	77.8	22.9	130	1.9	129	186	131	41.5
PG-1150	0.67	0.03	35.4	<0.01	0.31	0.17	0.03	39.7	0.09	19	10	3.7	<0.1	6.8	0.5	5	8.3	385	5.7
Soil*	61.74	2.86		3.67		14.17	2.68	3.44	12.11	92	280			67	4.8	203	28	348	17

* Continental crust composition [36].

toxicity characteristic leaching procedure (TCLP) was carried out [30]. In addition, the leachates were analysed by both alpha spectrometry and ICP-MS techniques.

Natural radionuclides were measured in both raw materials and samples by high-resolution low-background gamma spectrometry with a hyper-pure germanium detector (HPGe) with a carbon window, through the following energies: ^{210}Pb (46.5 keV), ^{234}Th (63.3 keV), ^{226}Ra (via 352 keV of ^{214}Pb) and ^{40}K (1460 keV). The activity concentrations in leachates obtained during the TCLP method were measured by alpha-particle spectrometry with ion-implanted Si detectors. U-isotopes, Th-isotopes, and ^{210}Po were isolated by a tributilphosphate sequential extraction method [31]. Furthermore, the activity concentration index (I) was determined to evaluate the potential radiological risks [32]. The effective radium activity is defined as the ^{222}Rn concentration generated by ^{226}Ra contained inside the material and transported through its pores. According to Krisyuk [33], it is calculated by multiplying the ^{226}Ra concentration (Bq kg^{-1}) by the effective radium activity, which is determined under specific experimental conditions from the growth curves of radon inside a closed chamber.

3. Results and discussion

3.1. Material characterisation

Fig. 1 shows the results of the particle size analysis of the PG used in this study. It revealed an asymmetric particle size distribution with a wide range of particle sizes. Two different populations were observed (see Fig. 1); the main fraction presents the major population around 50 μm, and the second population is around 4 μm. According to the particle size, the clay fraction of the total particles (particle size below 2 μm) is below 20%, the silt fraction (particle size between 50 and 2 μm) is 40%, and the sand fraction (particle size above 50 μm) is 40%.

The textural characterisation (sand, silt, and clay) of the clay sample using the pipette method showed a great plasticity, according to the high clay minerals fraction (51.6%). Consequently, a considerable amount of water (12 wt%) was required to shape the tiles easily. The silt and sand fractions of the clay were 23.9% and 24.5% respectively.

In accordance with the mineralogical analysis (Fig. 2a), the crystalline components of the clay were quartz (SiO_2), kaolinite ($Al_2Si_2O_5(OH)_4$), illite ($KAl_2Si_4O_{10}(OH)_2$), goethite ($FeO(OH)$) and gibbsite ($Al(OH)_3$). The XRD pattern of the PG (Fig. 2b) confirmed it was exclusively of the mineral phase gypsum ($CaSO_4{\cdot}2H_2O$). Fig. 3 shows a sequence of diffraction patterns of the clayed material, with 0, 5, 7.5, and 10 wt% PG, sintered at 1150 °C. As shown in Fig. 3, after the firing process, the peaks associated with clay minerals (kaolinite and illite) disappear because of the destruction of the crystalline structure at 450–900 °C. Above 900 °C, new mineral phases such as mullite ($3Al_2O_3{\cdot}2SiO_2$) appear, due to the crystallisation process. As a consequence of mullite formation, a reduction in the intensities of the XRD peaks of quartz was observed (Fig. 3). Moreover, after the firing process, hematite was identified, and goethite disappeared. The iron from the goethite decomposition, and the release of iron by illite during the breakdown of its mineral structure, form the new mineral phase detected; hematite [34]. Furthermore, the XRD patterns show the formation of new mineral phases with the addition of PG (Fig. 3), such as the calcium silicates wollastonite ($CaSiO_3$) and anorthite ($CaAl_2Si_2O_8$). The gibbsite decomposition, and the release of aluminium by kaolinite and illite together with the Ca from the PG form the anorthite. The intensities of the peaks associated with these calcium silicates (wollastonite and anorthite) increase with the percentage of gypsum in

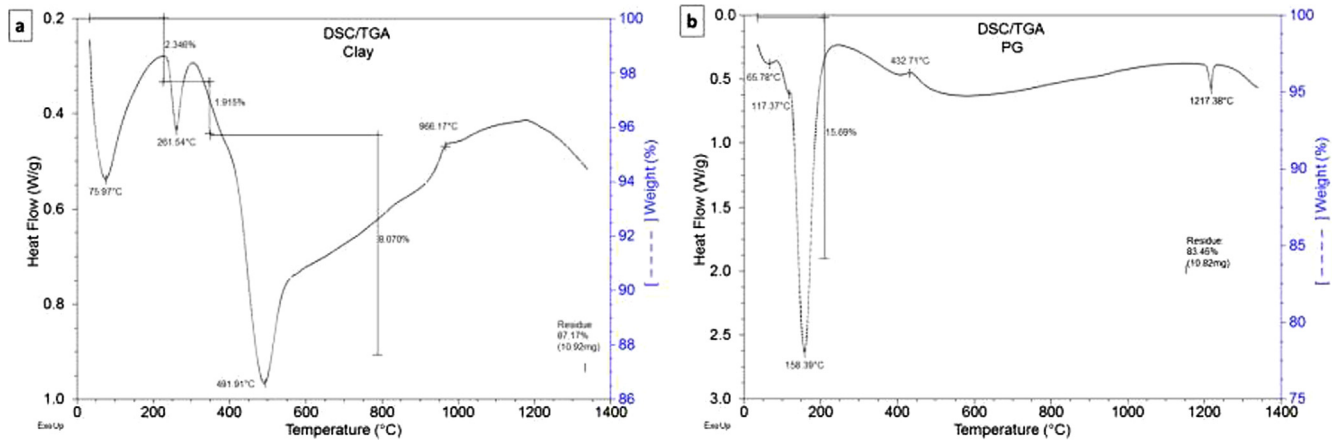

Fig. 4. DSC/TGA curves (25–1350 °C, 10 °C min^{-1}) of the raw materials: (a) clay and (b) phosphogypsum.

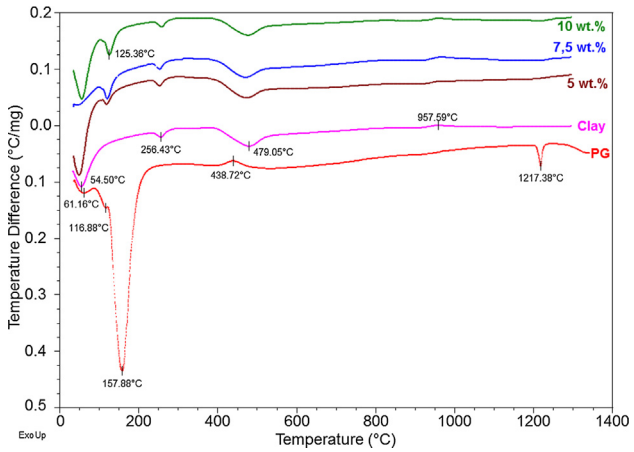

Fig. 5. DSC curves (25–1350 °C, 10 °C min^{-1}) of the clay, PG and the different mixtures of clay with phosphogypsum added (wt%): (a) clay, (b) 5, (c) 7.5, (d) 10 and (e) PG..

the specimens. PG has an important content of calcium sulphate, a nucleating agent that may have influenced the crystallisation of mineral phases like wollastonite [35].

In agreement with the XRD results, the chemical analysis showed that PG is mainly composed of SO_3 (52.2 wt%) and CaO (30.6 wt%); similar results have been reported in other studies [15,36]. The main trace elements identified in PG are (in order of abundance), Sr, Cr, Cu, Mn, Zn, Pb, and Zr; all present, however, in concentrations smaller than in unperturbed soils [37]. The chemical analysis (Table 2) shows that clay is composed of high amounts of silica (48.82 wt%), alumina (27.67 wt%), and iron oxide (7.09 wt%) and potassium oxide (2.55 wt%). These results are in accordance with the mineral composition obtained previously by XRD analysis. Regarding the trace impurities, Mn, Cu, Zn, Cr, Ni, Sr, Pb, and Co were detected in clay. Some trace elements (Cu, Zn, Cr, and Pb) are present in concentrations higher than in uncontaminated soils [36]. On the other hand, the mean valued obtained in this study for major, trace metals and radionuclide are in accordance with the obtained for several previous studies carried out in the same place [3,8,38–40]. The DSC/TGA analysis of PG and clay are represented in Fig. 4. The losses on ignition (at 1150 °C) were 16.55 wt% and 12.83 wt%, for PG and clay respectively. Fig. 4a shows the DSC/TGA curves for the clay, in which one exothermic and four endothermic peaks were identified. The first endothermic peak at ~76 °C is associated with a weight loss of 2%, which corresponds to the endothermic evaporation of unbound water. Another endothermic peak at ~262 °C with a weight loss of 1% corresponds to the thermal decomposition of non-volatile organic compounds, the volatilisation of lighter organic fragments, and especially to the decomposition of Al and Fe hydroxides (gibbsite and goethite, respectively). The largest mass loss (8%) occurs at ~492 °C, due to the endothermic dehydroxylation of clay minerals as, the decomposition of kaolinite, and the loss of structural water of illite. The third peak at ~966 °C is exothermic and it is characteristic of the crystallisation of mullite. Finally, an endothermic descent at ~1200 °C is related to the formation of a liquid phase derived from the feldspar component and the silica released [41].

The thermal behaviour of PG (Fig. 4b) shows five areas of weight change; one exothermic and four endothermic peaks. The first endothermic area at ~66 °C is associated with the partial dehydration of gypsum ($CaSO_4{\cdot}2H_2O$) to give hemihydrate gypsum ($CaSO_4{\cdot}½H_2O$). In the second endothermic peak at ~117 °C, the dehydration of the hemihydrate gypsum begins. In the third endothermic effect at ~158 °C, the main mass loss (10%) occurred due to the complete removal of crystallisation water and the consequent formation of soluble anhydrite III ($CaSO_4$ III). The fourth thermal effect, an exothermic peak at ~433 °C, is related to the transformation of soluble anhydrite III into insoluble anhydrite II. Finally, an endothermic peak at ~1217 °C takes place due to the total decomposition of calcium sulphate into calcium oxide (CaO) and sulphur dioxide (SO_2). The results are in concordance with the results obtained by XRD and with other researchers [42,43].

Fig. 5 shows the DTA curves of mixtures of clay with 0, 5, 7.5, and 10 wt% of PG. The thermal behaviour of the mixtures was similar to that of the clay, although with the addition of PG, some areas associated with the thermal behaviour of gypsum appeared. Moreover, the chemical composition of the clay was altered with the addition of PG, changing the reactions that occurred during the firing process. The endothermic peaks around 262 °C and 492 °C were reduced in samples with added PG due to the amount of clay substituted by PG.

FESEM observations of polished surfaces of the ceramic samples fired at 1150 °C are shown in Fig. 6. In 0-1150 sample (Fig. 6a), a dense matrix is observed; porosity mainly consists of fine closed pores (<5 μm) distributed throughout the clay matrix, with some open porosity composed by interconnected irregular channels with a size below 5 μm. The addition of 5 wt% PG leads to fired samples with a lower amount of fine closed porosity (Fig. 6b), but a slightly higher number of larger isolated pores (>10 μm) that form coarse closed porosity due to the release of gaseous SiO_2 during the ther-

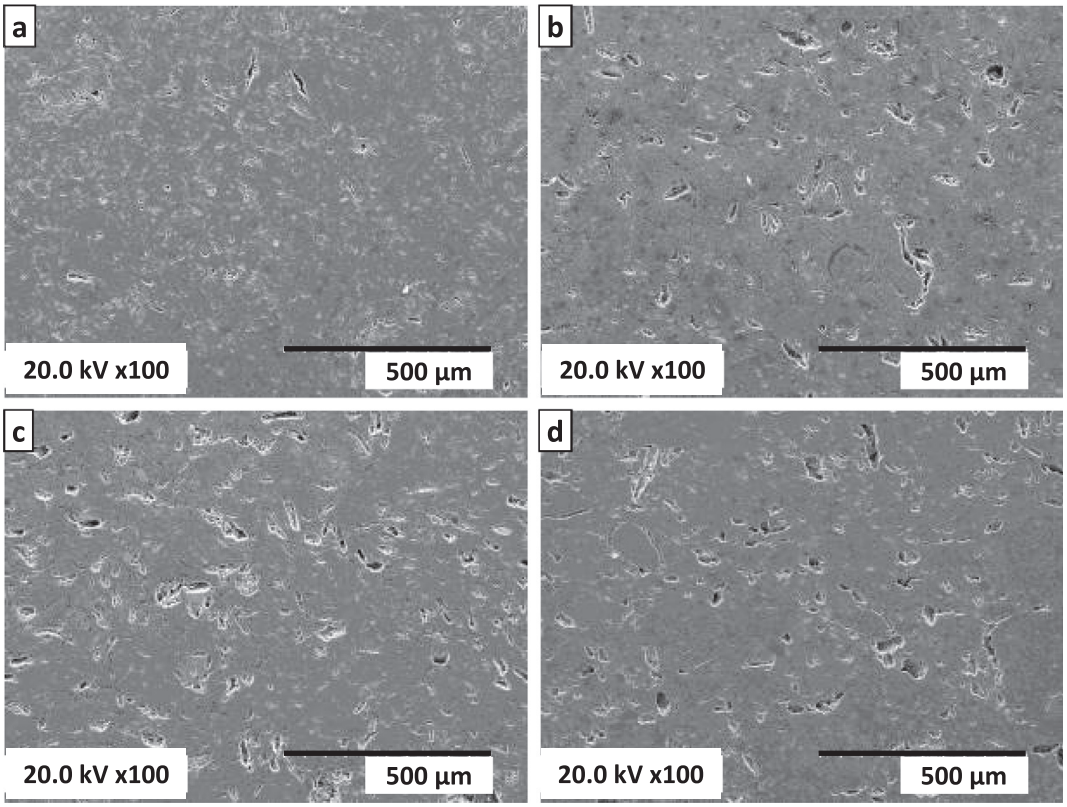

Fig. 6. FESEM observations on polished surfaces of the ceramics fired at 1150 °C: a) clay without PG addition (0-1150); b) clay + 5 wt% PG (5-1150); c) clay + 7.5 wt% PG (7.5-1150); d) clay + 10 wt% PG (10-1150).

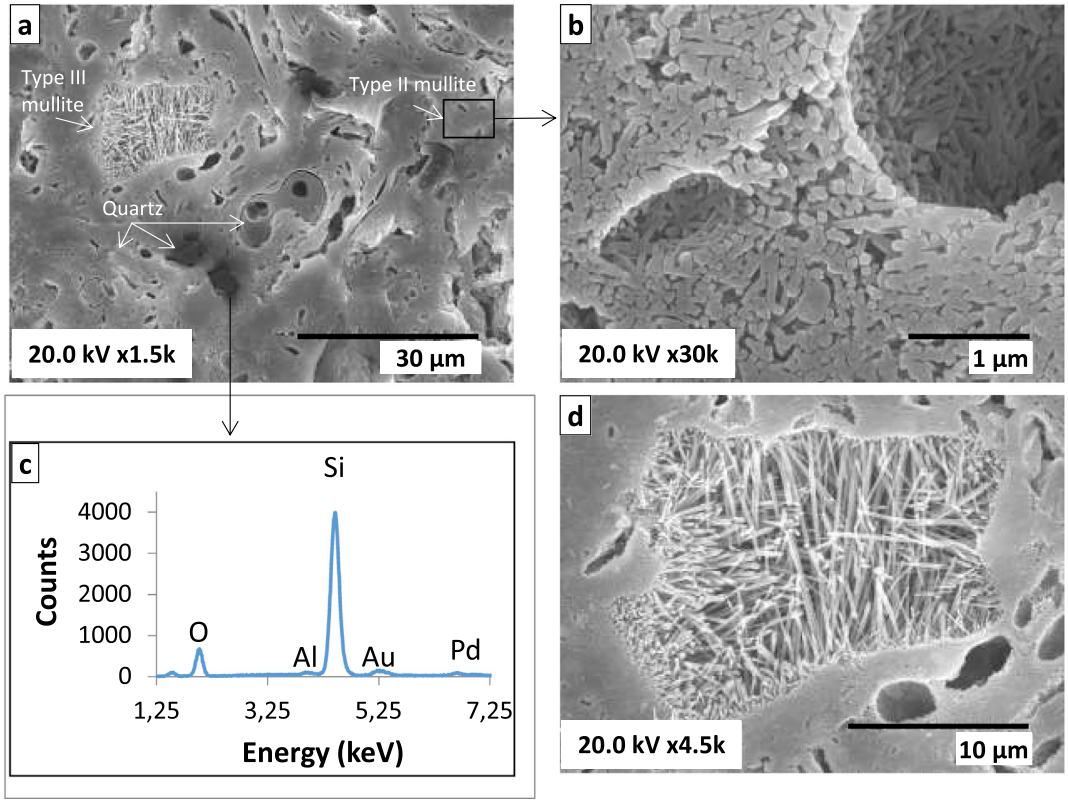

Fig. 7. FESEM/SE images of fresh fractured, etched ceramic prepared from clay without PG addition and fired at 1150 °C (0-115): a) general microstructure; b) Type II secondary mullite matrix; c) EDS analysis of quartz particles; and d) Type III secondary mullite crystals.

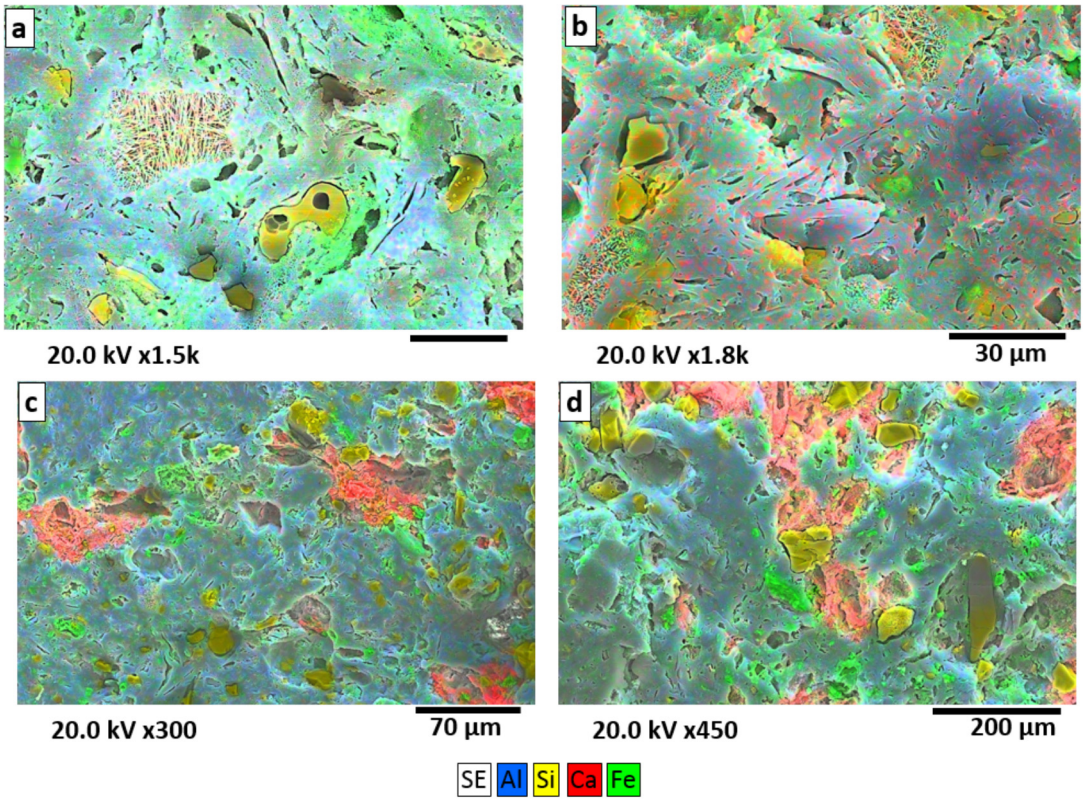

Fig. 8. FESEM/SE images and elemental mappings of Si, Al, Ca and Fe in ceramics fired at 1150 °C: a) clay without PG addition (0-1150); b) clay + 5 wt.% PG (5-1150); c) clay + 7.5 wt.% PG (7.5-1150); d) clay + 10 wt.% PG (10-1150).

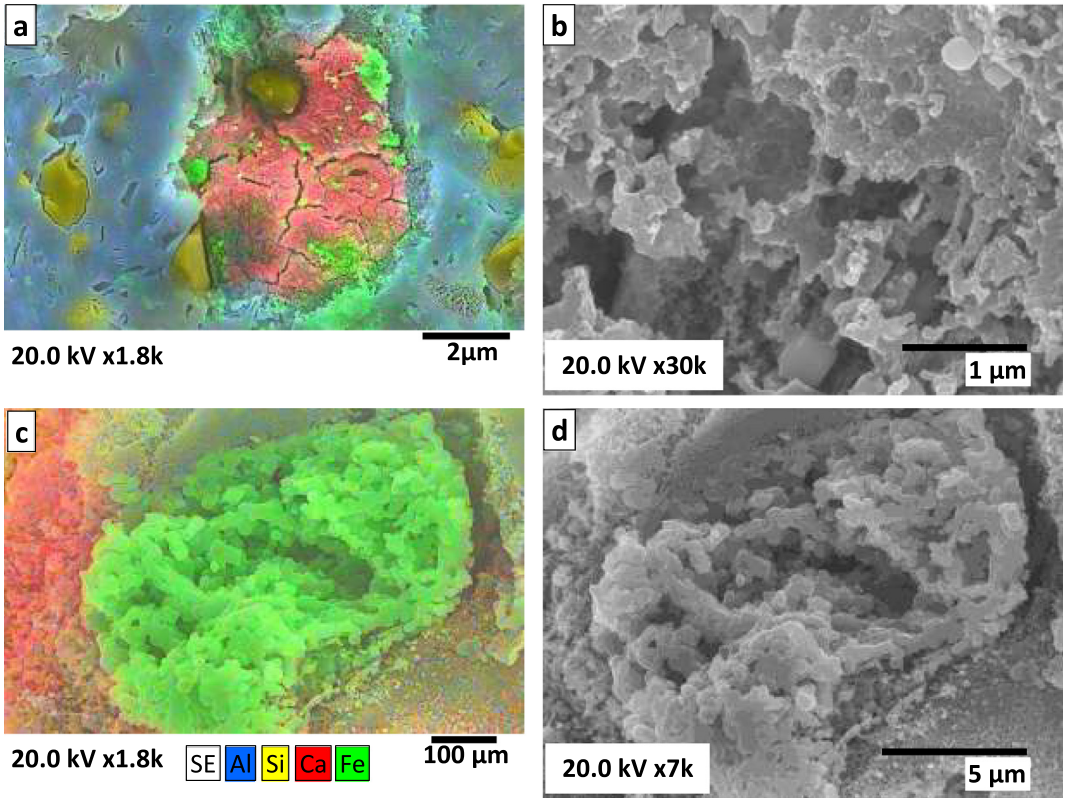

Fig. 9. FESEM/SE images and elemental mappings of Si, Al, Ca and Fe in fired ceramics at 1150 °C, prepared from clay and different percentages of PG: a) and b) clay + 5 wt.% PG (5-1150); c) and d) clay + 7.5 wt.% PG (7.5-1150).

Table 3
Sintering properties (water absorption, WA; apparent porosity, AP; and bulk density, BD), linear shrinkage (LS), and bending strength (BS) results of tiles fired at different temperatures. Results show average values of 3 measurements.

	WA (wt%)	AP (%)	LS (%)	BD ($g \cdot cm^{-3}$)	BS (MPa)	Classification EN 14411*	Classification ANSI A137.1**
Fired at 950 °C							
0-950	19.87 ± 0.07	34.8 ± 0.7	3.0 ± 0.1	1.75 ± 0.02	6.7 ± 0.2	–	P4
5-950	18.52 ± 0.08	32.6 ± 0.9	3.0 ± 0.1	1.76 ± 0.03	5.8 ± 0.3	–	P4
7.5-950	18.70 ± 0.09	32.9 ± 0.8	3.3 ± 0.1	1.76 ± 0.02	5.2 ± 0.2	–	P4
10-950	19.23 ± 0.07	33.7 ± 1.0	3.1 ± 0.1	1.75 ± 0.02	4.6 ± 0.2	–	P4
Fired at 1050 °C							
0-1050	10.31 ± 0.04	21.9 ± 0.7	8.1 ± 0.1	2.07 ± 0.02	24.5 ± 0.5	BIII	P4
5-1050	9.85 ± 0.05	21.3 ± 0.8	8.9 ± 0.2	2.06 ± 0.03	25.3 ± 0.4	BIIb	P4
7.5-1050	9.49 ± 0.04	19.9 ± 0.7	8.8 ± 0.2	2.09 ± 0.03	24.2 ± 0.4	BIIb	P4
10-1050	8.61 ± 0.06	18.3 ± 0.9	9.0 ± 0.2	2.12 ± 0.03	21.1 ± 0.5	BIIb	P4
Fired at 1150 °C							
0-1150	3.21 ± 0.03	7.5 ± 0.2	12.0 ± 0.3	2.34 ± 0.02	32.4 ± 0.7	BIIa	P3
5-1150	2.93 ± 0.05	6.8 ± 0.3	11.1 ± 0.3	2.30 ± 0.03	34.5 ± 0.8	BIb	P2
7.5-1150	2.99 ± 0.05	6.9 ± 0.5	10.7 ± 0.4	2.25 ± 0.02	32.6 ± 0.7	BIb	P2
10-1150	4.68 ± 0.07	10.2 ± 1.9	10.8 ± 0.4	2.17 ± 0.04	25.4 ± 0.9	BIIa	P3

* Classified according to the water absorption coefficient (WA) and the bending strength resistance (BS).
** Classified according to the water absorption coefficient (WA) and the forming method.

mal decomposition of PG. The coarse closed porosity increases as the amount of PG in the initial composition increases (Fig. 6c; d), which is likely to be responsible for the reduction observed in bending strength, given that these pores can act as stress concentrators and facilitate fracture [44].

Fig. 7 shows micrographs taken on etched surfaces of the ceramic 0-1150. Etching with HF solution leads to the partial removal of the glass phase, and consequently the different crystalline phases detected by XRD are highlighted. The microstructure is comprised of a dense matrix in which diverse crystals and regions with distinctive morphology are included (Fig. 7a). High magnification observation allows the dense matrix to be recognised, consisting of small prismatic crystals showing a high aspect ratio (3–10:1), which correspond to Type II secondary mullite derived from a kaolinite/illite mixture (Fig. 7b). The potassium and iron in the clay composition develop a liquid phase at low temperatures, which facilitates the growth of these crystals, so they achieve higher aspect ratios than mullite crystals formed from pure kaolinite relicts [45]. Moreover, quartz crystals are also observed in the matrix that are clearly identified by EDS analysis (Fig. 7c), as well as crystalline regions consisting of mullite needles with very high aspect ratio (30–40:1) that correspond to Type III secondary mullite, likely derived from areas where kaolinite, illite, and quartz are finely mixed. In such areas, mullite crystals are enclosed in a more fluid liquid, which promotes the growth of longer crystals (Fig. 7d).

The elemental mappings of Si, Al, Ca, and Fe related to samples fired at 1150 °C are shown in Fig. 8. The hematite and Ca-enriched phases are identified by colour dissimilarities caused by different concentrations of these ions in each of the observed crystalline phases. As expected, the prevalence of these Ca- or Fe-enriched phases is higher with greater additions of PG. The addition of greater amounts of PG gives rise to negligible changes in the microstructure after firing in terms of the morphology of the matrix, quartz, and secondary mullite crystals, as shown in Fig. 8b where the microstructure of the ceramic 5-1150 is shown. Nevertheless, the greatest effect of adding PG is the occurrence of neo-formation phases embedded in the ceramic matrix.

Fig. 9(a–b) show elemental mapping and a SEM/secondary electron (SE) image corresponding to a Ca-enriched region in the sample 5-1150. It is likely that these regions are developed from areas where pure PG was located in the green body. As a result of gas release during the thermal decomposition of PG, these Ca-enriched regions show higher porosity than the ceramic matrix. Although the existence of anorthite and wollastonite has been detected by XRD, it is not possible to identify the crystals corresponding to each of these phases by SEM as the region shows a homogeneous morphology consisting of granular aggregates. Regarding the hematite phase, Fig. 9(c–d) show elemental mapping and a SEM/SE image corresponding to hematite crystals showing globular habit, observed in the sample 7.5-1150.

3.2. Technological properties

The technological properties of fired tiles shown in Table 3 indicate that water absorption (WA) is a function of firing temperature, due to an increase of amorphous silica with sintering temperature and thus formation of mullite [46]. The amorphous silica and alumina are liberated when the kaolinite structure is broken, around 500 °C, and disappear when mullite is crystallised at 950 °C. The WA was reduced with the addition of PG for all temperatures, in agreement with the SEM study, but for 10-1150, the WA increased. The amorphous silica, which forms mullite during the sintering process, serves as a binder for the fine particles of PG, occupying the spaces between the granules. Hence, greater PG additions reduce the WA in the ceramic bodies by the increasing of interconnected pores.

In the same way, the apparent porosity (AP) decreases with the concentration of PG and especially with the increase of firing temperature. Both WA and AP are directly related to the open porosity, and therefore both present the same behaviour [43,47]. WA is an important property because it is related to the effective realisation of the sintering process by the liquid phase. In terms of freeze–thaw cycles and stain resistance, low values of WA and AP are advantageous. Moreover, lower values of WA signify less drying time.

The sintering behaviour has indicated that the linear shrinkage (LS) is directly connected with firing temperature (Table 3). As mentioned previously, higher temperatures mean better sintering and consequently better properties: lower AP and WA. The results for LS are consistent with those observed for AP and WA, because LS behaviour is inversely related to WA and AP. The maximum shrinkage values were obtained at 1150 °C (LS ≈ 12); almost four times higher than at 950 °C (LS ≈ 3). These LS results were related to the greater densification of the ceramic bodies with increased firing temperatures.

Interestingly, different trends were seen with the addition of PG in the ceramic bodies fired at different temperatures. At 950 °C, the

Table 4
Activity concentrations (Bq kg^{-1}) of raw materials (PG and clay), the mixtures (5, 7.5, and 10 wt% PG), and ceramic bodies. The activity concentration index "I" was calculated.

	^{210}Pb	^{234}Th	^{226}Ra (^{214}Pb)	^{228}Th (^{208}Tl)	^{228}Ra (^{228}Ac)	^{40}K	"I"
Raw materials and mixtures							
PG[a]	723 ± 24	92 ± 6	1054 ± 32	13 ± 3	11 ± 4	59 ± 7	N.M.
Clay[a]	53 ± 4	57 ± 7	55 ± 3	80 ± 3	83 ± 3	504 ± 14	N.M.
5 wt%[a]	73 ± 5	53 ± 5	101 ± 4	78 ± 4	75 ± 3	457 ± 21	N.M.
7.5 wt%[a]	94 ± 6	48 ± 5	127 ± 4	82 ± 4	83 ± 5	440 ± 21	N.M.
10 wt%[a]	120 ± 7	52 ± 5	159 ± 5	78 ± 5	74 ± 5	449 ± 22	N.M.
Fired at 950 °C							
0-950[b]	54 ± 4	65 ± 4	75 ± 3	103 ± 4	99 ± 4	608 ± 22	0.78
5-950[b]	86 ± 7	72 ± 6	134 ± 5	95 ± 5	97 ± 5	533 ± 24	0.95
7.5-950[b]	137 ± 8	67 ± 6	172 ± 6	93 ± 5	96 ± 5	538 ± 25	1.07
10-950[b]	139 ± 8	64 ± 6	192 ± 6	99 ± 5	97 ± 6	552 ± 26	1.15
Fired at 1050 °C							
0-1050[b]	53 ± 5	55 ± 5	71 ± 3	100 ± 5	98 ± 5	576 ± 24	0.76
5-1050[b]	113 ± 6	75 ± 8	146 ± 4	105 ± 3	103 ± 4	658 ± 18	0.88
7.5-1050[b]	115 ± 6	64 ± 5	167 ± 5	96 ± 5	89 ± 5	556 ± 23	1.04
10-1050[b]	139 ± 5	67 ± 4	202 ± 6	93 ± 4	94 ± 4	556 ± 19	1.17
Fired at 1150 °C							
0-1150[b]	71 ± 7	75 ± 10	81 ± 3	108 ± 4	112 ± 5	624 ± 20	0.85
5-1150[b]	110 ± 8	63 ± 11	139 ± 4	105 ± 4	99 ± 5	558 ± 21	0.98
7.5-1150[b]	130 ± 9	81 ± 11	177 ± 5	100 ± 4	105 ± 5	628 ± 29	1.15
10-1150[b]	157 ± 9	88 ± 11	215 ± 6	103 ± 4	106 ± 5	565 ± 19	1.26
PG-1150[b]	666 ± 19	97 ± 14	1313 ± 30	13 ± 3	15 ± 4	52 ± 12	4.45

N.M. not measured.
[a] Before firing process.
[b] After firing process.

LS remained constant with increasing PG; at 1050 °C, the LS increased slightly with increasing PG; and at 1150 °C, the LS decreased slightly with increasing PG. As expected, the LS of ceramic bodies is a function of the firing temperature and, to a lesser degree, the PG content. In terms of the resistance of ceramic bodies, lower LS values are better to avoid internal defects such as cracking or other similar faults during firing. LS is associated with the liquid phase formation during sintering; this is good for all properties. A lower LS signifies greater preservation of the size of the ceramic piece after the firing process. According to the LS results, the addition of PG reduced the shrinkage and deformation of the material during the firing process due to two factors; the occupation of pores by PG particles, and the non-plastic behaviour of the PG compared to the clay. Both factors reduced the great plasticity in the clay and thus improved the stability of the material.

The results for bulk density (BD) were in accordance with the LS behaviour, as both properties are directly related. At 950 °C, the BD values remained practically constant with different percentages of PG; at 1050 °C, the BD increased slightly with increasing PG (Table 3); and at 1150 °C, the BD decreased with increasing PG.

Table 3 shows that bending strength (BS) values were similar or even higher in ceramic bodies fired at 1050 and 1150 °C with additions of up to 7.5 wt% PG than in the reference materials (0-1150). This occurred due to the denser, lower-porosity material obtained at these temperatures. The incorporation of PG produces two effects, on the one hand, it favors the formation of wollastonite and the reduction of plasticity in the clay that improves the microstructure and increases the resistance, and on the other hand, the PG decomposition releases gases causing closed porosity (>10 μm) that weakens the structure.

The best resistance results were obtained from the samples 5-1050 and 5-1150; the decrease in the AP caused by the low addition of PG, in particular the reduction of plasticity in the clay and fine closed pores in the fired material, improved the sintering behaviour of the ceramic bodies during the firing process and their resistance to rupture. On the other hand, a 10 wt% addition of PG reduced the resistance of the bodies; the rupture tension values were lower because the AP increases because coarse closed and interconnected open porosity increased (Table 3). In general, the addition of PG decreases the bending strength due to the coarse closed porosity increased. On the other hand, low percentages of PG and high sintering temperatures increased the resistance probably because in those cases the beneficial effect of the formation of wollastonite prevails over the resistance reduction due to the development of closed pores

On the other hand, the BS in samples fired at 950 °C decreased with increasing PG concentrations. All of them presented lower values than the reference material (0-950). This diminution of BS was produced by the increasing of interconnected pores and consequently by the increasing of fracture points. Moreover, the decrease in BS values in samples fired at 950 °C with added PG can be attributed to the fact that quartz does not participate in the formation of new phases at sintering temperatures lower than 1000 °C, instead acting as fracture points.

Ceramic tiles are classified in the standards EN 14411 [48] and ANSI A137.1 [49] according to the WA coefficient and the BS. The European Norm EN 14411 [48] establishes the following classifications: BIb requires 0.5–3% WA and 30 MPa BS; BIIa requires 3–6% WA and 22 MPa BS; BIIb requires 18 MPa BS and 6–10% WA; and finally, BIII requires ≥10% WA and 15 MPa BS. All samples fired at 950 °C had WA values above 10%, belonging to the BIII group, but the minimum resistance value was not reached. The specimens fired at 1050 °C are classified in the BIIb group, with BS values above 18 MPa (between 21.1 and 25.3 MPa) and WA results between 8 and 10%. Samples 5-1150 and 7.5-1150 belong to the BIb group, with WA below 3% (WA ≈ 2.9%) and BS above 30 MPa (32.6–34.5 MPa). Finally, sample 10-1150 is classified in the BIIa group, with a WA value of 4.7% and a BS above 22 MPa (25.4 MPa).

Furthermore, the American National Standard ANSI A137.1 [49] establishes a classification based on the WA and the forming method, in our case by pressing. The specimens 5-1150 and 7.5-1150 are classified as vitreous (0.5–3% WA) with a BS above the 32 MPa requirement, and belong to the P2 group. The sample 10-1150 is classified in the P3 group, a semi-vitreous ceramic (3–7% WA) with a BS above the 22 MPa requirement for floor tiles. Finally, the samples fired at 950 and 1050 °C are classified as

Table 5
Leachability concentrations of metals obtained by TCLP test analysed by ICP-OES. Transfer factor (%) of metal into TCLP extractant.

	Si mg L^{-1}	Na mg L^{-1}	S mg L^{-1}	Mg mg L^{-1}	P mg L^{-1}	Al mg L^{-1}	K mg L^{-1}	Ca mg L^{-1}	Fe mg L^{-1}	Cr μg L^{-1}	Mn mg L^{-1}	Ni μg L^{-1}	Co μg L^{-1}	Zn μg L^{-1}	As μg L^{-1}	Cd μg L^{-1}	Cu μg L^{-1}	Sr μg L^{-1}	Pb μg L^{-1}	Ba mg L^{-1}
Clay[a]	3.6	0.13	0.8	7.2	0.06	0.4	4.4	33.7	0.05	<20	0.91	15	24	465	<30	<2	88	330	30	1.83
	(0.02)	(0.2)	(12)	(2.6)	(0.4)	(0.00)	(0.5)	(40.4)	(0.00)	(–)	(7.1)	(0.4)	(2.4)	(6.5)	(–)	(–)	(1.0)	(10.6)	(1.7)	(–)
PG[a]	0.3	0.12	664	0.2	11.3	2.3	1.7	850	0.04	<20	0.01	29	<2	131	<30	16	28	3670	20	0.03
	(0.15)	(1.2)	(3.8)	(6.0)	(10.3)	(4.6)	(17.0)	(8.3)	(0.15)	(–)	(3.3)	(18.1)	(–)	(45.2)	(–)	(–)	(6.9)	(22.6)	(7.7)	(–)
0-950[b]	8.4	0.14	1	2.9	0.02	1.9	39	3.9	0.06	<20	0.12	16	4	257	<30	<2	67	60	<10	0.40
	(0.05)	(0.2)	(8.5)	(1.2)	(0.1)	(0.02)	(4.4)	(5.3)	(0.00)	(–)	(0.9)	(0.4)	(0.4)	(3.4)	(–)	(–)	(0.9)	(2.2)	(–)	(–)
10-950[b]	11.4	0.12	72	2.3	0.05	4.1	36.7	91.1	0.08	30	0.10	14	3	259	<30	<2	58	150	<10	0.04
	(0.08)	(0.2)	(11.3)	(0.9)	(0.2)	(0.05)	(4.6)	(6.6)	(0.00)	(0.4)	(0.8)	(0.4)	(0.3)	(4.4)	(–)	(–)	(1.1)	(2.6)	(–)	(–)
0-1050[b]	7.2	0.14	2	1.8	0.03	1.3	18.1	4.2	1.98	30	0.10	18	4	110	<30	<2	60	40	<10	0.20
	(0.04)	(0.2)	(3.9)	(0.8)	(0.1)	(0.02)	(2.5)	(4.9)	(0.08)	(0.4)	(0.8)	(0.5)	(0.4)	(1.5)	(–)	(–)	(0.8)	(1.5)	(–)	(–)
10-1050[b]	11.1	0.13	60	1.7	0.04	5.2	15.2	74	2.12	40	0.10	17	4	88	<30	<2	48	100	<10	0.18
	(0.08)	(0.2)	(4.5)	(0.6)	(0.2)	(0.06)	(2.3)	(4.2)	(0.02)	(0.5)	(0.8)	(0.4)	(0.4)	(1.2)	(–)	(–)	(0.6)	(2.2)	(–)	(–)
0-1150[b]	5.3	0.13	3	1.1	<0.02	5.5	14.3	4.5	2.65	80	0.08	37	4	100	<30	<2	54	30	<10	0.16
	(0.04)	(0.2)	(4.5)	(0.3)	(–)	(0.06)	(1.4)	(4.8)	(0.10)	(0.9)	(0.5)	(0.9)	(0.3)	(1.4)	(–)	(–)	(0.6)	(0.9)	(–)	(–)
5-1150[b]	6.8	0.12	37	1.1	<0.02	5.9	10.5	52.9	1.38	70	0.07	25	3	60	<30	<2	49	120	<10	0.16
	(0.05)	(0.2)	(9.0)	(0.3)	(–)	(0.07)	(1.1)	(6.6)	(0.05)	(0.6)	(0.5)	(0.6)	(0.3)	(0.8)	(–)	(–)	(0.6)	(2.5)	(–)	(–)
7.5-1150[b]	8.7	0.14	49	1.6	0.07	7.1	12.5	70.6	1.76	90	0.08	26	3	64	<30	<2	33	160	<10	0.18
	(0.07)	(0.2)	(7.4)	(0.5)	(0.4)	(0.09)	(1.3)	(5.8)	(0.07)	(0.7)	(0.6)	(0.7)	(0.3)	(1.1)	(–)	(–)	(0.6)	(2.9)	(–)	(–)
10-1150[b]	10.7	0.14	41	1.6	0.03	7.1	11.9	65.1	2.32	70	0.10	27	4	62	<30	<2	50	150	<10	0.18
	(0.08)	(0.2)	(5.4)	(0.5)	(0.1)	(0.10)	(1.2)	(4.1)	(0.08)	(0.7)	(0.7)	(0.7)	(0.4)	(1.0)	(–)	(–)	(0.5)	(2.3)	(–)	(–)
Liquid 1	1.2	<0.02	<1	<0.1	<0.02	<0.1	2.2	<0.1	0.02	<20	<0.01	<2	<2	8	<30	<2	<10	<10	<10	<0.02
U.S.EPA	–	–	–	–	–	–	–	–	–	5000	–	–	–	25,000	5000	1000	–	–	5000	100

Limit values given in the U.S. EPA 40 CFR 261.24 standard [51].
Liquid 1 used according U.S. EPA TCLP test [29].
[a] Before firing process.
[b] After firing process.

Table 6
Average activity concentration (mBq L^{-1}) of leaching obtained by TCLP test and analysed by alpha spectrometry. Transfer factor (%) of radionuclides into TCLP extractant.

	^{238}U		^{234}U		^{232}Th		^{230}Th		^{228}Th		^{210}Po	
	mBq L^{-1}	%	mBq L^{-1}	%	mBq L^{-1}	%	mBq L^{-1}	%	mBq L^{-1}	%	mBq L^{-1}	%
PG[a]	200 ± 12	4.32	170 ± 14	3.68	50 ± 23	9.17	110 ± 33	0.21	49 ± 31	7.67	15 ± 4	0.04
Clay[a]	40 ± 10	1.41	40 ± 10	1.41	250 ± 51	6.00	50 ± 27	1.83	57 ± 30	1.42	102 ± 12	3.81
0-950[b]	50 ± 10	1.53	10 ± 8	0.31	80 ± 21	1.61	70 ± 10	1.86	13 ± 8	0.27	19 ± 8	0.72
10-950[b]	100 ± 10	3.12	60 ± 10	1.87	60 ± 20	1.24	40 ± 3	0.42	10 ± 7	0.21	27 ± 5	0.39
0-1050[b]	50 ± 10	1.34	10 ± 3	0.27	50 ± 10	0.89	60 ± 10	1.49	19 ± 3	0.35	15 ± 3	0.44
10-1050[b]	50 ± 5	1.58	30 ± 10	0.95	30 ± 3	0.60	40 ± 3	0.56	24 ± 5	0.46	21 ± 4	0.38
0-1150[b]	40 ± 6	1.07	10 ± 3	0.27	30 ± 3	0.53	30 ± 3	0.74	22 ± 3	0.41	8 ± 3	0.22
5-1150[b]	30 ± 3	0.95	10 ± 3	0.32	13 ± 3	0.26	40 ± 10	0.56	34 ± 3	0.65	11 ± 6	0.19
7.5-1150[b]	40 ± 3	0.98	30 ± 10	0.74	10 ± 4	0.19	40 ± 3	0.45	32 ± 10	0.64	18 ± 6	0.28
10-1150[b]	40 ± 10	0.91	10 ± 3	0.23	10 ± 3	0.19	30 ± 5	0.28	33 ± 9	0.65	13 ± 9	0.17
Liquid 1	4 ± 2	N.M.	8 ± 2	N.M.	5 ± 2	N.M.	8 ± 3	N.M.	8 ± 3	N.M.	11 ± 2	N.M.

N.M. not measured.
Liquid 1 used according U.S. EPA TCLP test [29].
[a] Before firing process.
[b] After firing process.

non-vitreous (7–20% WA) and belong to the P4 group, however the samples fired at 950 °C did not meet the minimum value for wall tiles (BS >15 MPa).

3.3. Environmental study

The radioactive characterisation of the ceramic bodies and raw materials should be the first step to evaluating the radiological impact associated with the use of PG. According to Table 4, PG shows a ^{226}Ra concentration higher than the safety threshold (1000 Bq kg^{-1}) for NORMs, established by UNSCEAR in 1988 [50]. The main radionuclides are ^{226}Ra and ^{210}Pb, with activity values of 1080 and 720 Bq kg^{-1} respectively. The radionuclides in clay are in secular equilibrium with their daughters and show similar concentrations to the average worldwide values for soils. The average activity concentrations in soil – reported by UNSCEAR in 2008 [51] – of ^{226}Ra, ^{228}Ra, and ^{40}K are 32, 25, and 412 Bq kg^{-1} respectively, and Radiation Protection 112 [32] established a control threshold of 40 Bq kg^{-1} of ^{226}Ra and ^{228}Ra and 400 Bq kg^{-1} of ^{40}K. Moreover, the activity concentration of the ceramic bodies shows that the radionuclides ^{226}Ra and ^{210}Pb increased with increasing PG (Table 4). The concentrations of ^{228}Ra, ^{228}Th, and ^{234}Th were constant for all mixtures and firing temperatures. On the other hand, the activity concentration of ^{40}K decreased with the increase of PG, since the concentration in PG is 10 times lower than in clay.

In order to evaluate the environmental impact of adding PG to building materials, the activity concentration index (I) was calculated according to Eq. (2):

$$I = \frac{C_{226_{Ra}}}{300} + \frac{C_{232_{Th}}}{200} + \frac{C_{40_K}}{3000} \quad (2)$$

where C(^{226}Ra), C(^{232}Th), and C(^{40}K) are the respective activities for ^{226}Ra, ^{232}Th, and ^{40}K in the ceramic bodies, expressed in Bq kg^{-1}. International regulations establish that this index should not exceed a value of 6 for superficial materials [32]. Values under this limit prevent the external dose received by occupants in buildings using this material from exceeding the established limit of 1 mSv $year^{-1}$ [52]. The index I (Table 4) shows that PG could be used as additive in the manufacture of ceramic bodies, since the values obtained are clearly lower than the limit for superficial materials (I < 6). Furthermore, the results of this index were significantly lowered in comparison with the results achieved in other studies using other additives in ceramics [43,48,53]. Moreover, sample analysis confirmed that, for all firing temperatures studied, samples containing up to 5 wt% PG could be used even as bulk material, as the index I does not exceed the limit of 1 established for bulk materials [32]. Hence, in accordance with the limits established in the standards, tiles manufactured exclusively with PG are permitted for use as superficial materials.

The radon characteristics of the ceramic bodies were analysed since raw materials with high ^{226}Ra activity concentrations have been used. The effective radium activity is the main characteristic to be studied, and it is defined as the fraction of ^{222}Rn produced by the ^{226}Ra contained inside the grains that is able to escape into the pores within the material. The measurement of the effective radium concentration from the ceramic bodies was calculated according to the method developed by López-Coto et al. [33]; i.e. the product of the ^{226}Ra concentration (Bq kg^{-1}) and the emanation factor, determined under specific experimental conditions. The radium effective concentrations were below the detection limit of 5 Bq kg^{-1}; lower than ordinary construction materials such as cement (10 Bq kg^{-1}) [32]. To assess the contribution of building materials to indoor radon concentrations, a specific scenario was considered; in this case a standard room (5 × 5 × 2.5 m) with an air exchange rate of 0.5 h^{-1} was assumed. The contribution to indoor radon concentration in the room due to emissions – using worst-case conditions – was below 4 Bq m^{-3}. This value is in accordance with the limit of 100 Bq m^{-3} established by the Commission Recommendation 90/143/Euratom [54] for new construction materials.

The potential environmental impact of the ceramic bodies was also evaluated by TCLP tests [30]. This method classifies waste as hazardous or non-hazardous based on toxicity. If the extract from a representative sample contains any of the contaminants listed in U.S. EPA 40 CFR 261.24 [55] at a concentration equal to or greater than the respective value given, it is classified as hazardous. The results of the TCLP tests are shown in Table 5, which permit the ceramic bodies to be considered as non-hazardous waste; all of the leachates were present in values lower than the regulatory levels listed in the U.S. EPA [55]. The leached concentrations of Cr, Zn, As, Cd, Pb, and Ba exhibited a direct relation to the initial concentrations in the raw materials (PG and clay) and the percentage of each in the mix. After 18 h of leaching, the amounts of leachates detected from the new ceramic bodies were below the allowed U.S. EPA values of 5 mg L^{-1} for Cr, As, and Pb; 25 mg L^{-1} for Zn; and 1 mg L^{-1} for Cd and Ba.

These results indicate that the incorporation of PG into ceramics meets the requirements for recycling this hazardous waste; the levels are below the ecotoxicity limits, ensuring that the use of this

material will not impact the environment. Moreover, the mobility of metals (Table 5) studied by the transfer factor (%) show that the sintering process contributes to the encapsulation and stabilisation of metals in the ceramic matrix, avoiding the biodisponibility in the leachates. This fact can be observed due to the drastic reduction of transfer factor values after the firing process. Most of the transfer factor values in fired samples were below 1%, showing that the metals largely do not leach out.

Furthermore, the radiological environmental impact of the leachates obtained by TCLP tests were analysed according to the activity concentration and the radionuclide mobility (Table 6). The results shown the low activity concentration in the leachates obtained. The highest activity concentration, of ^{238}U, was obtained from the sample 10-950 (0.10 Bq L^{-1}); below the provisional guideline value of 10 Bq L^{-1} introduced by the World Health Organisation (WHO) for total activity content of uranium in drinking water [56], and clearly lower than values recorded for continental waters (which typically range between 0.005 and 0.5 Bq L^{-1}) [57]. The leachates show a ^{234}U activity concentration between 0.01 and 0.06 Bq L^{-1}, rising to the maximum value in 10-950. This value is two orders of magnitude lower than the reference level established by the WHO (1 Bq L^{-1}). The U-isotopes concentration in leachates is quite low and would therefore have negligible environmental impact.

According to thorium radionuclides, the concentrations of Th-isotopes show the lowest value in leachates from 0 to 950 (0.05 Bq L^{-1} of ^{232}Th), and the maximum value in leachates from 10 to 1150 (0.62 Bq L^{-1} of ^{228}Th). The activity concentration of ^{230}Th presented values between these. These results were of same order of magnitude as those typical of continental waters [57], and lower than the guidance levels for thorium radionuclides in drinking water (1 Bq L^{-1}) [56], thus their potential radiological impact is negligible.

Furthermore, the highest ^{210}Po activity concentration was 27.3 mBq L^{-1} for 10-950 and the lowest was 7.0 mBq L^{-1} for 0-1150. The results were lower than the average values obtained for ^{210}Po in continental water (0.050–1 Bq L^{-1}) [56,58] and below the WHO threshold for this radionuclide in drinking water of 0.1 Bq L^{-1}.

Finally, the leachates all showed a similar ^{226}Ra concentration of 0.04–0.1 Bq L^{-1}; this range is one order of magnitude lower than the guidance level of 1 Bq L^{-1} in drinking water [56].

According to these results, the effective dose equivalent received by the public due to leachates was not significant, since the natural radioactivity levels measured were lower than the representative worldwide averages and guidance levels. The radionuclide mobility was studied based on the transfer factors. Table 6 shows the transfer factors (%) of the natural radionuclides measured. The results show that radioisotopes will not leach out after the sintering process, which immobilises the radionuclides in the ceramic matrix.

4. Conclusions

The present work has demonstrated that phosphogypsum can be successfully used as additive in ceramics. It should be pointed out that developing applications that use PG in high percentage is not technologically suitable. In the majority of the uses of PG this is incorporated in small proportions (around 10%) as our methodology proposes for the ceramics. This method is one more option to help in the storing elimination of this waste.

The addition of PG has a beneficial role in the sintering behaviour, decreasing both the apparent porosity and water absorption. All technological properties are associated with the formation of mullite, above 950 °C. As shown in the results, higher temperatures mean better sintering and consequently better properties: lower porosity and water absorption, and as consequence higher mechanical resistance.

The linear shrinkage increases with temperature and with the amount of PG added, of samples fired at 950 and 1050 °C; and at 1150 °C, the LS decreased slightly with increasing PG, reducing the shrinkage and deformation of the material during the firing process. This is due to the small particles of PG that occupy the pores; the PG has a non-plastic behaviour compared to the clay used. Both factors reduced the great plasticity of the clay and improved the stability of the material.

The results of the mechanical properties study show that the incorporation of PG does not cause any significant variation in bending strength values; the results are similar, and in some cases improved, compared to the reference samples. The addition up to 5 wt% PG increases the rupture resistance; samples with 7.5 wt% PG showed similar results, and the incorporation of 10 wt% PG reduced the bending strength.

The obtained results are in line with other studies performed on the incorporation of wastes to ceramic matrix, which conclude that wastes can be included as additives in the composition ceramic building materials without lead to high variations and even increasing the technological properties of the fired materials.

Based on the environmental risk study, the environmental impact is negligible. The metals and radionuclides are immobilised in the ceramic matrix, avoiding biodisponibility in the leachates. The radon level and the external dose received by occupants in buildings using this material do not exceed the established limits.

Considering all the results it can be concluded that the ideal conditions for the combination of this clay with the largest volume of immobilised PG are: the addition of 7.5% by weight of PG at the sintering temperature of 1050 °C.

Declarations of interest

None.

Acknowledgements

This research has been partially supported by the Spanish Government Department of Science and Technology (MINECO), by the project "Fluxes of radionuclides emitted by the PG piles located at Huelva; assessment of the dispersion, radiological risks and remediation proposals" (Ref.: CTM2015-68628-R). PhD student M. Contreras would like to express his gratitude for the research contract granted to him through the Fellowship Training Program of the University Teaching Staff (Ref.: AP2010-2746), financed by the Spanish Ministry of Education, Culture and Sport (MECD). This research has been partially supported by São Paulo Research Foundation (FAPESP) (Ref.: 2013/07296-2) in the Center for the Development of Functional Materials (CDMF), Laboratory of Ceramic Materials (LaMaC/UNESP), Campus of Presidente Prudente, São Paulo, Brazil.

References

[1] P.M. Rutherford, M.J. Dudas, R.A. Samek, Environmental impacts of phosphogypsum, Sci. Total Environ. 149 (1994) 1–38.
[2] H. Tayibi, M. Choura, F.A. López, F.J. Alguacil, A. López-Delgado, Environmental impact and management of phospho-gypsum, J. Environ. Manage. 90 (8) (2009) 2377–2386.
[3] J.P. Bolívar, J.E. Martín, R. García-Tenorio, J.P. Pérez-Moreno, J.L. Mas, Behaviour and fluxes of natural radionuclides in the production process of a phosphoric acid plant, Appl. Radiat. Isot. 67 (2009) 345–356.
[4] J. Yang, W. Liu, L. Zhang, B. Xiao, Preparation of load-bearing building materials from autoclaved phosphogypsum, Constr. Build. Mater. 23 (2009) 687–693.

[5] A.B. Parreira, A.R.K. Kobayashi Jr., O.B. Silvestre, Influence of Portland cement type on unconfined compressive strength and linear expansion of cement stabilized phosphogypsum, J. Environ. Eng. 129 (2003) 956–960.
[6] G.H. Kim, A study on establishing quality certification of standardization for waste gypsum recycling, in: Final report, Incheon (Korea), Korea Environment Corporation, Division of research and development, 2010, Report No.: KECO2010-RE17-31, Contract No.: 11-1480000-001132-01.
[7] U.N.D.P. Ifa, The Fertilizer Industry's Manufacturing Process and Environmental Issue, Report 28, UN Publications, Paris, 1998.
[8] J.L. Mas, E.G. San Miguel, J.P. Bolívar, F. Vaca, J.P. Pérez-Moreno, An assay on the effect of preliminary restoration tasks applied to a large TENORM wastes disposal in the south-west of Spain, Sci. Total Environ. 364 (2006) 55–66.
[9] R. Pérez-López, A.M. Álvarez-Valero, J.M. Nieto, Changes in mobility of toxic elements during the production of phosphoric acid in the fertilizer industry of Huelva (SW Spain) and environmental impact of phosphogypsum wastes, J. Hazard. Mater. 148 (2007) 745–750.
[10] J.P. Bolívar, R. García-Tenorio, M. García-León, Enhancement of natural radioactivity in soils and salt-marshes surrounding a non-nuclear industrial complex, Sci. Total Environ. 173 (1995) 125–135.
[11] V.A. Mymrin, K.P. Alekseev, A. Nagalli, R.E. Catai, C.A. Romano, Hazardous phosphor-gypsum chemical waste as a principal component in environmentally friendly construction materials, J. Environ. Chem. Eng. 3 (2015) 2611–2618.
[12] N. Degirmenci, Utilization of phosphogypsum as raw and calcined material in manufacturing of building products, Construct. Build. Mater. 22 (8) (2008) 1857–1862.
[13] S. Kumar, Fly ash–lime–phosphogypsum hollow blocks for walls and partitions, Build. Environ. 38 (2) (2003) 291–295.
[14] I. Akın Altun, Y. Sert, Utilization of weathered phosphogypsum as set retarder in Portland cement, Cem. Concr. Res. 34 (4) (2004) 677–680.
[15] M. Contreras, R. Pérez-López, M.J. Gázquez, V. Morales-Flórez, A. Santos, L. Esquivias, J.P. Bolívar, Fractionation and fluxes of metals and radionuclides during the recycling process of phosphogypsum wastes applied to mineral CO_2 sequestration, Waste Manage. 45 (2015) 412–419.
[16] C. Cárdenas-Escudero, V. Morales-Flórez, R. Pérez-López, A. Santos, L. Esquivias, Procedure to use phosphogypsum industrial waste for mineral CO_2 sequestration, J. Hazard. Mater. 196 (2011) 431–435.
[17] H. Youqiang, Comprehensive Utilization of Phosphor-gypsum as Waste Residue in Phosphate Fertilizer Industry. Co-production of Sulfuric Acid and Cement from Phosphor-gypsum, Guizhou Chemical Industry, China, 2010.
[18] M. Garg, N. Jain, Waste gypsum from intermediate dye industries for production of building materials, Constr. Build. Mater. 24 (2010) 1632–1637.
[19] F.A. López, M. Gázquez, F.J. Alguacil, J.P. Bolívar, I. García-Díaz, I. López-Coto, Microencapsulation of phosphogypsum into a sulfur polymer matrix: physicochemical and radiological characterization, J. Hazard. Mater. 19 (1) (2011) 234–245.
[20] A.P. Godinho-Castro, R.C. Testolin, L. Janke, A.X.R. Corrêa, C.M. Radetski, Incorporation of gypsum waste in ceramic block production: proposal for a minimal battery of tests to evaluate technical and environmental viability of this recycling process, Waste Manage. 32 (2012) 153–157.
[21] J. Zhou, Z. Shu, L.I. Tiantian, Y.U. Dongxue, Z. Sheng, Y. Wang, Novel fabrication route for non-fired ceramic tiles only using gypsum, Ceram. Int. 41 (2015) 9193–9198.
[22] S.R. Teixeira, A.E. Souza, M.A.L. Nobre, Physical and mechanical properties of ceramics from clays of the west of S. Paulo State, Brazil, Cerâmica 50 (2004) 268–273.
[23] M.A. Nuñez-Granados, F. Díaz del Olmo, J.M. Recio, Espejo, Alteraciones caoliníticas sobre rocas plutónicas de Sierra Morena Occidenteal (Sierra de Aracena, Huelva), Geogaceta 25 (1999) 151–154.
[24] A. Klute, Methods of Soil Analysis: Physical and Mineralogical Methods Part 1, second ed., Soil Science Society of America Book Series, Madison, Wisconsin, 1986. No. 9 (Part 1) Agronomy Series.
[25] ISO 10545-3:1997, Ceramic Tiles – Part 3: Determination of Water Absorption, Apparent Porosity, Apparent Relative Density and Bulk Density, International Organization for Standardization, Geneva, 1997.
[26] ASTM C373-14, Standard Test Method for Water Absorption, Bulk Density, Apparent Porosity, and Apparent Specific Gravity of Fired Whiteware Products, Ceramic Tiles, and Glass Tiles, ASTM International, West Conshohocken, PA, 2014.
[27] ASTM C326-9, Standard Test Method for Drying and Firing Shrinkages of Ceramic Whiteware Clays, ASTM International, West Conshohocken, PA, 2009.
[28] ISO 10545-4:2014, Ceramic Tiles – Part 4: Determination of Modulus of Rupture and Breaking Strength, International Organization for Standardization, Geneva, 2014.
[29] ASTM C674-13, Standard Test Methods for Flexural Strength Properties of Ceramic Whiteware Materials, ASTM International, West Conshohocken, PA, 2018.
[30] U.S. EPA SW-846, Test Methods for Evaluating Solid Waste Physical Chemical Methods, U.S. Environmental Protection Agency, Washington DC, 1997.
[31] R.L. Lozano, J.P. Bolívar, E.G. San Miguel, R. García-Tenorio, M.J. Gázquez, An accurate method to measure alpha-emitting natural radionuclides in atmospheric filters: application in two NORM industries, Nucl. Instrum. Methods A 659 (2011) 557–568.
[32] Radiation protection 112, Radiological Protection Principles concerning the Natural Radioactivity of Building Materials, European Commission, Stuk, 1999.
[33] Z.E. Krisyuk, Radiation Background of Premises, Energoatomizdat Publ., Moscow, 1989 (120 pp., in Russian).
[34] U. Schwertmann, R.M. Taylor, Iron oxides, in: J.B. Dixon, S.B. Weed (Eds.), Mineral in soil environments, second ed., Soil Science Society of America Book Series, Madison, Wisconsin, 1989, pp. 379–438.
[35] A.J. Lewry, J. Williamson, The setting of gypsum plaster, Part III: the effect of additive and impurities, J. Mat. Sci. 29 (1994) 6085–6090.
[36] J.E. Martín, R. García-Tenorio, M.A. Respaldiza, M.A. Ontalba, J.P. Bolívar, M.F. da Silva, TTPIXE analysis of phosphate rocks and phosphogypsum, Appl. Radiat. Isot. 50 (1999) 445–449.
[37] R.L. Rudnick, S. Gao, Composition of the continental crust, in: H.D. Holland, K. K. Turekian (Eds.), Treatise of Geochemistry, Vol. 3, Elsevier, 2003, pp. 1–64.
[38] J.P. Bolívar, R. García-Tenorio, M. García-León, On the fractionation of natural radioactivity in the production of phosphoric acid by the wet acid method, J. Radioanal. Nucl. Chem. 214 (1996) 77–88.
[39] J.L. Mas, J.P. Bolívar, R. García-Tenorio, Radioactivity of phosphogypsum in South-West of Spain, Radiat. Prot. Dosimetry 76 (1998) 85–189.
[40] E. Borrego, J.L. Mas, J.E. Martín, J.P. Bolívar, F. Vaca, J.L. Aguado, Radioactivity levels in aerosol particles surrounding a large TENORM waste repository after application of preliminary restoration work, Sci. Total Environ 377 (2007) 27–35.
[41] M. Contreras, M.I. Martín, M.J. Gázquez, M. Romero, J.P. Bolívar, Valorisation of ilmenite mud waste in the manufacture of commercial ceramic, Constr. Build. Mater. 72 (2014) 31–40.
[42] T.S. Sebbahi, M.L. Ould-Chameikh, F. Sahban, J. Aride, L. Benarafa, L. Belkbir, Thermal behaviour of Moroccan phosphogypsum, Thermo. Chim. Acta. 302 (1–2) (1997) 69–75.
[43] D.L. Hudson-Lamb, C.A. Strydom, J.H. Potgieter, The thermal dehydration of natural gypsum and pure calcium sulphate dihydrate (gypsum), Thermo. Chim. Acta 282 (283) (1996) 483–492.
[44] M. Romero, J.M. Pérez, Relation between the microstructure and technological properties of porcelain stoneware: a review, Mater. Constr. 65 (2015) e065, https://doi.org/10.3989/mc.2015.05915.
[45] J. Martín-Márquez, J.M. Rincón, M. Romero, Mullite development on firing in porcelain stoneware bodies, J. Eur. Ceram. Soc. 30 (2010) 1599–1607.
[46] C.M.F. Vieira, E.T.A. Souza, S.N. Monteiro, Influence of grog addition on a clay body used in red ceramic products, Ind. Ceram. 24 (2004) 85–89.
[47] M. Contreras, M.I. Martín, M.J. Gázquez, M. Romero, J.P. Bolívar, Manufacture of ceramic bodies by using a mud waste from the TiO_2 pigment industry, Key Eng. Mater. 663 (2016) 75–85.
[48] EN 14411:2004, Ceramic tiles – Definitions, classifications, characteristics and marking (ISO 13006:1998, modified), International Organization for Standardization, Geneva, 2004.
[49] ANSI A137.1, American National Standard Specifications for Ceramic Tile, American National Standard Institute, Washington DC, 2017.
[50] United Nations Scientific Committee on the effects of Atomic Radiation (UNSCEAR), Sources, effects and risks of ionizing radiation, in: Report to the General Assembly, with annexes, United Nations, New York, 1988.
[51] United Nations Scientific Committee on the effects of Atomic Radiation (UNSCEAR), Sources and Effects of Ionizing Radiation, Annex B, United Nations, New York, 2008.
[52] K. Kovler, Radiological constraints of using building materials and industrial by-products, Constr. Build. Mater. 23 (2009) 246–253.
[53] K. Kovler, G. Haquin, V. Manasherov, E. Neman, N. Lavi, Limitation of radionuclides concentration in building materials available in Israel, Build. Environ. 37 (2002) 531–537.
[54] 90/143/Euratom, Commission Recommendation of 21 February 1990 on the protection of the public against indoor exposure to radon, 1990.
[55] U.S. EPA, Test Methods for Identification and Listing of Hazardous Waste, Subpart c: Characteristics of Hazardous Waste, Section 261.24: Toxicity Characteristic, U.S. Environmental Protection Agency, Washington DC, 2011.
[56] WHO, Guidelines for Drinking-water Quality, fourth ed., World Health Organization, Geneva, 2015, p. 2011.
[57] J.L. Mas, M. García-León, R. García-Tenorio, J.P. Bolívar, Radionuclide concentrations in water, in: E. Nollet (Ed.), Radionuclide Concentrations in Food and the Environment, first ed., CRC Press, Boca Raton, FL, 2006, pp. 59–113.
[58] B.R.R. Persson, ^{210}Po and ^{210}Pb in the terrestrial environment, Curr. Adv. Environ. Sci. 2 (1) (2014) 22–37.